Helios: a New Type of Linear/Helical Undulator

P. Elleaume

ESRF, BP 220, F-38043 Grenoble, France

A new class of undulator capable of producing linear and/or helical polarization is described. The magnetic field, power, spectral flux, brilliance and interactions with the electron beam of such undulators are discussed. The case of Helios, an undulator presently installed on the ESRF, is discussed in detail.

Keywords: undulators; wigglers; X-ray sources; insertion devices; polarization.

1. Introduction

Generating circularly polarized radiation from insertion devices (IDs) has been the subject of intense activity in recent years. The first undulator producing circularly polarized radiation was used in a free-electron laser (Elias & Madey, 1979). The undulator essentially consisted of a superconducting double-helix coil. Helical undulators were later recognized to have high potential in generating synchrotron radiation (Kincaid, 1977). A new device called a crossed undulator has been independently proposed by Moissev, Nikitin & Fedorov (1978) and Kim (1984). The crossed undulator consists of two planar undulator sections. The magnetic fields from each section are orthogonal to one other. The two sections are separated by a drift space or a three-pole dispersive section. One problem associated with the crossed undulator is the rapid flipping of the polarization *versus* the photon energy. As a result, the overall maximum circular polarization rate does not coincide with the maximum intensity and strongly depends on the emittance of the electron beam. A permanent magnet design of a helical undulator was proposed by Onuki (1986) which suffered from a large magnetic gap requirement. Yamamoto & Kitamura (1987) proposed the use of a permanent magnet ellipsoidal magnetic field to produce a helically polarized wiggler type of radiation. The magnetic design consists of a strong vertical magnetic field combined with a small horizontal magnetic field of identical period. Partially circularly polarized radiation is produced along the axis of the device. Such a device has been successfully used on the accumulator ring at KEK. Simultaneously, the asymmetric wiggler was proposed by Goulon, Elleaume & Raoux (1987). The asymmetric wiggler consists of a non-sinusoidal planar magnetic field designed in such a way that the source points seen by an observer looking along the axis do not have the same absolute value (as occurs in a conventional planar wiggler). As a result, circularly polarized radiation is produced at sufficiently high photon energy. In terms of circularly polarized flux produced per unit length of magnet array, an asymmetric wiggler is less efficient than an elliptical wiggler, typically by a factor of 2–4. The brilliance (flux per unit transverse phase space) of the asymmetric wiggler placed on a low-emittance medium- or low-energy machine can be significantly reduced compared with an ellipsoidal wiggler. Nevertheless, the magnetic design is much simpler. Asymmetric wigglers have been successfully installed on DORIS (Pfluger & Heintze, 1990), SuperACO and ESRF. Elleaume (1990) proposed the construction of a linear/helical undulator by combining a non-symmetrical magnet array. The upper magnet array produces a horizontal sinusoidal magnetic field while the lower magnet array produces a vertical field. The polarization is controlled by longitudinally displacing one magnet array with respect to the other one. This concept resulted in the construction of Helios which will be detailed in this article. The advantage of Helios is the use of a flat vacuum chamber (as for any conventional undulator) and of harmonics 1, 3 and 5 by combining equal or different horizontal and vertical magnetic fields. The main drawback is the deflection experienced by an electron beam injected along the axis of the device. Such a deflection is absent from the design of Diviacco & Walker (1990), which can only be used on the fundamental at a fixed polarization. A more advanced design has been proposed by Sasaki (1993), which generates a significantly higher magnetic field. The price that has to be paid is a variation of the energy of the fundamental with the selected state of polarization and a significant mechanical complexity. Such a device has been successfully tested on the JSR ring at JAERI. A similar device is being commissioned at SSRL (Carr, 1993).

Finally, one should not forget that a number of attempts have been made to transform the linear polarization from a planar undulator into circular polarization with the VUV or X-ray equivalent of a quarter wave plate (commonly available in the visible range of the spectrum). Several beamlines are presently being designed in this manner including the magnetic scattering beamline of the ESRF. A review of such beamlines is beyond the scope of this article.

A beamline of the ESRF is dedicated to the study of natural and magnetic dichroism in X-ray absorption spectroscopy (Elleaume *et al.*, 1991). An optimized source for such an application must provide a flexible polarization

in the photon energy range between 0.5 and 10 keV. A close collaboration with the scientists in charge of the beamline resulted in the design and manufacture of Helios, a new type of linear/helical undulator (Elleaume, 1990). In the course of the design a complete new study of several important topics was carried out, namely the heat load, polarization, flux and interactions with the stored electron beam. The results of these studies are presented in this paper together with their application to the specific case of Helios.

2. Magnetic field of Helios

Fig. 1 illustrates the magnetic design of Helios. It consists of three parts: the upstream and downstream undulator sections, and the chicane magnets. Both upstream and downstream undulators present nine periods of 85 mm. Each undulator consists of two magnet jaws. The upper (lower) jaw placed above (below) the electron beam generates the horizontal (vertical) magnetic field. The upper (lower) magnets from both undulators and from the chicane are rigidly attached to a stiff girder. The vertical positions of the upper and lower girders are not varied symmetrically with respect to the electron beam as in conventional undulators but can be moved independently of each other. In addition, the longitudinal position of the upper girder can be changed. The longitudinal displacement between the girders is called the phase. Variation of the phase results in a change of the ellipticity of the magnetic field between linear (phase = 0) and circular right (phase = period/4) or circular left (phase = −period/4). In the following, the phase φ is expressed in terms of the undulator period and varies between $-\pi$ and π. The vertical magnetic field from both undulators is identical whereas the horizontal field is reversed resulting in opposite circular polarization between the upstream and the downstream undulators. The chicane consists of magnet blocks placed at both extremities of the two undulator segments. They are shown shaded in Fig. 1. Because of the chicane, the electron propagates at a different angle in the two undulators. The angle between the two undulator

axes is variable between 200 and 300 μrad depending on the position of the upper and lower girders. This figure must be compared with $1/\gamma = 85$ μrad, the typical angle of emission of synchrotron radiation by 6 GeV electrons. The chicane has two purposes. First, it spatially dissociates the two beams with opposite polarization generated by the upstream and downstream undulator sections. Each beam is reflected on a separate mirror in the beamline. Both beams then re-coincide on the sample to be studied. A chopper wheel is placed close to the mirrors resulting in a fast periodic flipping of the polarization of the X-ray beam incident on the sample. The second purpose is to minimize the interaction with the electron beam stored in the storage ring (see §4). It is worth emphasizing that conventional undulators offer a single degree of freedom, namely the magnetic gap, which changes the peak magnetic field, whereas Helios offers three degrees of freedom which are remote controlled. In the following, the vertical distance between the upper (lower) magnet array and the electron axis will be called uhg (lhg) which stands for upper half gap (lower half gap). Note that uhg + lhg is the total gap between the upper and lower magnet arrays. uhg, lhg and φ are the three degrees of freedom. The combined use of these degrees of freedom allows the selection of any arbitrary elliptical magnetic field within the limitation of a maximum vertical (horizontal) peak magnetic field of 0.37 T (0.28 T). The useful range is between 10 mm (0.28 T) and 30 mm (0.034 T) for uhg and between 10 mm (0.37 T) and 40 mm (0.046 T) for lhg. Horizontal and vertical correction coils have been placed below the magnetic assemblies. These coils are intended to minimize a possible distortion of the closed-ring orbit when any one of the three parameters is changed. Helios has been assembled, measured and shimmed according to the standard ESRF procedure for the production of IDs (Chavanne et al., 1992). The final measured field integral was smaller than 30 μT m in both planes for any independent setting of the three degrees of freedom. This figure was obtained without current in the correction coils.
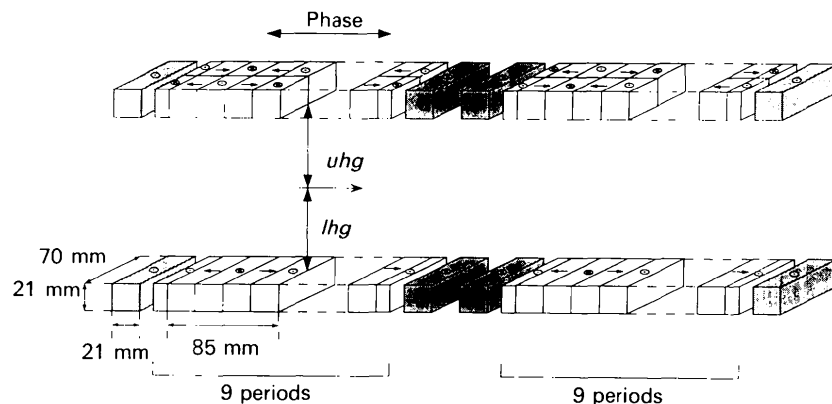
Figure 1
Magnetic design of Helios. The shaded magnets make up the chicane.

Fig. 2 presents the measured vertical and horizontal field for $uhg = lhg = 10$ mm and $\varphi = \pi/2$ together with the trajectory computed for a 6 GeV electron energy.

3. Power

3.1. General

The angle integrated power (kW) generated by a linear/helical device is

$$P = 1.266E^2 I \int_0^L (B_x^2 + B_z^2)\mathrm{d}s \tag{1}$$

where E is the electron energy (GeV), I is the electron current (A) and L is the length of the undulator (m). B_x and B_z (T) are the horizontal and vertical transverse components of the magnetic field at the longitudinal coordinate s. Assuming a periodic device of period λ_0 and magnetic gap g, the magnetic field can be viewed as a Fourier expansion of various harmonics. The most important components are those transverse to the electron beam. Moreover, because of the Maxwell equations, the magnetic field is largely dominated by the fundamental Fourier component. In the large majority of linear/helical undulators, the field is therefore purely sinusoidal and can be described by the vertical (horizontal) peak field $\hat{B}_z$ ($\hat{B}_x$) together with the phase φ between the two components. Then (1) reduces to

$$P = 0.633E^2 IL(\hat{B}_x^2 + \hat{B}_z^2). \tag{2}$$

The power density (W mrad^{-2}) can be computed by rewriting an equation from Schwinger (1949) as:

$$\mathrm{d}P/\mathrm{d}\theta_x \mathrm{d}\theta_z = 13.44 \times 10^{-3} E^4 ILJ(\psi_x, \psi_z)$$

$$J = \frac{1}{L}\int_0^L \frac{\left(\frac{\mathrm{d}\nu_x}{\mathrm{d}s}\right)^2 + \left(\frac{\mathrm{d}\nu_z}{\mathrm{d}s}\right)^2}{D^3} - \frac{\left(\frac{\mathrm{d}\nu_x^2}{\mathrm{d}s} + \frac{\mathrm{d}\nu_z^2}{\mathrm{d}s}\right)^2}{D^5} \mathrm{d}s \tag{3}$$

where J is in m^{-2}, and D, ν_x and ν_z are given by

$$D = (1 + \nu_x^2 + \nu_z^2)$$

$$\nu_x(s) = \frac{e}{mc}\int_{-\infty}^s B_z \mathrm{d}s - \gamma\psi_x$$

$$\nu_z(s) = \frac{e}{mc}\int_{-\infty}^s -B_x \mathrm{d}s - \gamma\psi_z \tag{4}$$

in which e and m are the electron charge and mass, c is the speed of light, γ is the electron energy divided by mc^2, and ψ_x and ψ_z are the horizontal and vertical angles of observation. ν_x and ν_z represent the horizontal and vertical components of the instantaneous angle between the electron velocity and the direction of observation in units of $1/\gamma$. In the general case (3) must be integrated numerically. There are two extreme cases of interest. If the field is planar, (3) reduces to the one given in Kim (1986). If the field is purely helicoidal and is observed on axis then J reduces to

$$J(0,0) = \left(\frac{2\pi}{\lambda_0}\right)^2 \frac{K^2}{(1 + K^2)^3} \tag{5}$$
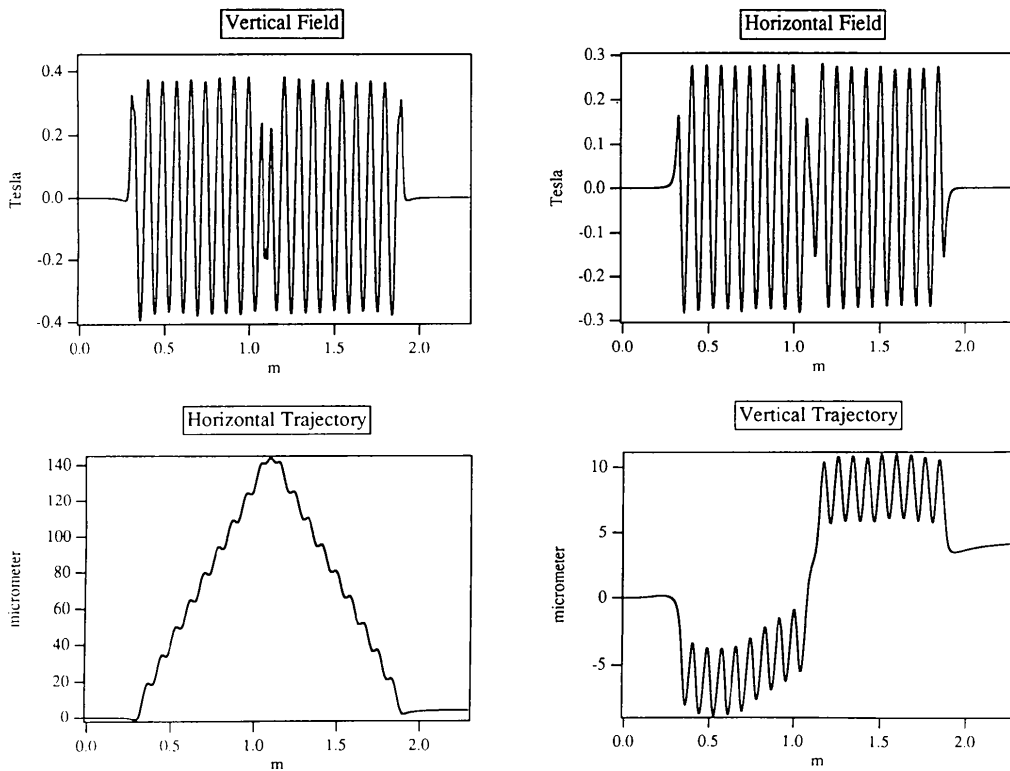
Figure 2

Measured vertical and horizontal field for $uhg = lhg = 10$ mm and $\varphi = \pi/2$ together with the trajectory computed for a 6 GeV electron energy.

Table 1

Peak magnetic field, angle integrated power from both segments and power density from a single undulator segment for various settings of *uhg* and *lhg*.

uhg (mm)	lhg (mm)	$\widehat{B}_x$ (T)	$\widehat{B}_z$ (T)	Power (kW)	Density (kW mrad^2)
10	10	0.26	0.35	1.38	11.0
15	15	0.14	0.24	0.56	7.0
20	20	0.08	0.16	0.24	4.5
25	25	0.05	0.11	0.10	2.9
30	30	0.03	0.07	0.04	1.8

where $K = 93.4\lambda_0\widehat{B}$ is the deflection parameter and λ_0 (m) is the undulator spatial period.

3.2. Application to Helios

Table 1 gives the total angle integrated power generated by both segments of Helios and the power density available on the axis of a single undulator segment. The electron energy is 6 GeV and the current is 200 mA.

4. Spectral flux, brilliance and polarization

4.1. General

The radiation spectrum generated by an electron beam crossing a linear/helical undulator consists of a series of narrow peaks. The peaks occur at photon energies $\varepsilon_n = n\varepsilon_1$ where n is an integer number (also called a harmonic number) and ε_1 is the energy of the fundamental peak. Along the axis of the electron beam, one essentially sees the odd harmonics (1, 3, 5) while off axis all harmonics contribute significantly. In the particular case of a perfectly helicoidal field, the harmonics higher than 1 vanish on axis. Consequently, the use of harmonics 3 and 5 with circular polarization is only possible by collecting the radiation off axis or by using unequal horizontal and vertical magnetic fields. This is the main reason why Helios was built with independent settings of *lhg* and *uhg*. A symmetric gap setting of the upper and lower girders would not allow the generation of significant circularly polarized flux on those harmonics whose photon energy range cannot be reached by the fundamental. There is a trade-off between flux on harmonics 3, 5, 7, *etc.* and circular polarization rate. Assuming a sinusoidal field, the nth harmonic of the undulator radiation spectrum observed on axis is

$$\varepsilon_n = \frac{0.0095nE^2}{\left(1 + \frac{K_x^2}{2} + \frac{K_z^2}{2}\right)\lambda_0} \qquad (6)$$

where K_x and K_z are the horizontal and vertical deflection parameters

$$K_x = 93.4\lambda_0\widehat{B}_x \quad K_z = 93.4\lambda_0\widehat{B}_z. \qquad (7)$$

The total spectral flux (integrated over all angles of emission) [photons s^{-1} (0.1%)$^{-1}$] generated on the odd harmonic on axis is:

$$F_n = 1.431 \times 10^{14} nNI\left(\frac{A^2 + B^2 + C^2}{1 + \frac{K_x^2}{2} + \frac{K_z^2}{2}}\right) \qquad (8)$$

where N is the number of undulator periods and A, B, C are given by

$$A = K_z J \quad B = K_x J\cos(\varphi) \quad C = K_x J\sin(\varphi) \qquad (9)$$

with

$$J = J_{(n+1)/2}(nD) - J_{(n-1)/2}(nD)$$

$$D = \frac{[K_x^4 + K_z^4 + 2K_x^2K_z^2\cos(2\varphi)]^{1/2}}{4\left(1 + \frac{K_x^2}{2} + \frac{K_z^2}{2}\right)} \qquad (10)$$

where φ is the phase between the horizontal and vertical sinusoidal fields and $J_n(x)$ is the nth order Bessel function of the variable x. Replacing K_x by zero in (8) and (9) gives the well known flux of a conventional planar undulator. Calling s_0 the flux given by (8), the three other Stokes components describing the polarization, s_1, s_2, s_3 (Born & Wolf, 1987), are given by

$$\frac{s_1}{s_0} = I_1 = \frac{-A^2 + B^2 + C^2}{A^2 + B^2 + C^2}$$

$$\frac{s_2}{s_0} = I_2 = \frac{2AB}{A^2 + B^2 + C^2}$$

$$\frac{s_3}{s_0} = I_3 = \frac{2AC}{A^2 + B^2 + C^2}. \qquad (11)$$

I_1 is the linear polarization rate associated with the horizontal and vertical planes of polarization. I_2 is the linear polarization rate associated with the two orthogonal axes making a 45° angle with respect to the horizontal and the vertical. I_3 is the circular polarization rate. If the field is planar and sinusoidal, (8) and (9) reduce to the well known result (Krinsky, 1983), in which case $I_3 = 0$.

So far I have assumed a filament electron beam and an observation point placed on axis at infinity. Consequently, the radiation is fully polarized and one can easily show from (11) that $I_1^2 + I_2^2 + I_3^2 = 1$. For a non-filament beam, the radiation in the harmonics is spread over a larger horizontal and vertical angle. Observed at a finite distance d in the beamline, the impact of the radiation at any harmonic energy given by (6) is a Gaussian ellipse with horizontal (vertical) r.m.s. beam size Σ_x (Σ_z),

$$\Sigma_x^2 = \varepsilon_x\left(\beta_x - 2\alpha_x d + d^2\frac{1 + \alpha_x^2}{\beta_x}\right) + \frac{\lambda}{4\pi}\left(\frac{L}{4\pi} + 4\pi\frac{d^2}{L}\right) \qquad (12)$$

where ε_x is the horizontal emittance of the electron beam, β_x is the horizontal beta function, $\alpha_x = -(1/2)(d\beta_x/ds)$. In the great majority of cases $\alpha_x = 0$. λ is the wavelength

Table 2

Dependence of the fundamental energy, total flux and polarization rates as a function of *uhg*, *lhg*, φ and harmonic number.

uhg (mm)	lhg (mm)	φ (rad)	Harmonic	Energy (keV)	Flux [photons s^{-1} (0.1%)$^{-1}$]	I_1	I_2	I_3
15	15	$\pi/2$	1	1.17	7.0×10^{14}	-0.33	0	0.95
15	15	0	1	1.17	4.8×10^{14}	-0.47	0.88	0
15	15	$-\pi/2$	1	1.17	7.0×10^{14}	-0.33	0	-0.95
10	10	$\pi/2$	1	0.58	8.8×10^{14}	-0.18	0	0.98
15	15	$\pi/2$	1	1.17	7.0×10^{14}	-0.33	0	0.95
20	20	$\pi/2$	1	1.96	5.0×10^{14}	-0.47	0	0.88
25	25	$\pi/2$	1	2.76	3.0×10^{14}	-0.59	0	0.80
30	30	$\pi/2$	1	3.35	1.7×10^{14}	-0.69	0	0.73
35	35	$\pi/2$	1	3.69	8.6×10^{13}	-0.75	0	0.66
10	10	0	1	0.58	5.0×10^{14}	-0.31	0	0.95
15	15	0	1	1.17	4.8×10^{14}	-0.47	0	0.88
20	20	0	1	1.96	4.0×10^{14}	-0.58	0	0.82
25	25	0	1	2.76	2.8×10^{14}	-0.66	0	0.75
30	30	0	1	3.35	1.7×10^{14}	-0.72	0	0.70
35	35	0	1	3.69	8.4×10^{13}	-0.76	0	0.65
15	15	$\pi/2$	3	3.50	1.2×10^{14}	-0.25	0	0.97
17	15	$\pi/2$	3	3.75	1.7×10^{14}	-0.38	0	0.93
20	15	$\pi/2$	3	4.00	2.0×10^{14}	-0.56	0	0.83
25	15	$\pi/2$	3	4.20	2.2×10^{14}	-0.80	0	0.60
30	15	$\pi/2$	3	4.27	2.2×10^{14}	-0.92	0	0.40

of the radiation and L the length of the undulator. The vertical size is obtained from (12) replacing x by z. Equation (12) presents two contributions, one from the electron beam and one from single-electron emission. Note that in most of the new generation of synchrotron sources single-electron emission dominates over the electron beam emittance contribution in the vertical plane, whereas the opposite is true in the horizontal plane. With a finite emittance, the polarization rates deviate somewhat from (11). One can define a total polarization rate R by

$$R^2 = I_1{}^2 + I_2{}^2 + I_3{}^2. \tag{13}$$

R is positive between 0 and 1. If $R = 1$ the radiation is said to be fully polarized whereas in the other extreme case of $R = 0$ the radiation is said to be fully depolarized. In the general case, the polarization rates must be determined numerically. For the majority of the sources optimized for small emittance, R stays close to 1.

The spectral brilliance B_n [photons s^{-1} (0.1%)$^{-1}$ mrad^{-2} mm^{-2}] on the nth odd harmonic can be computed in a similar way to that for a planar sinusoidal undulator:

$$B_n = F_n/(2\pi)^2 \Sigma_x \Sigma_z \Sigma_x' \Sigma_z' \tag{14}$$

in which Σ_x and Σ_x (Σ_x' and Σ_x') are the r.m.s. horizontal and vertical sizes (divergences) of the photon beam at the source. They are approximately given by

$$\Sigma_x^2 = \varepsilon_x \beta_x + \frac{\lambda L}{(4\pi)^2} \quad \Sigma_z^2 = \varepsilon_z \beta_z + \frac{\lambda L}{(4\pi)^2}$$

$$\Sigma_x'{}^2 = \frac{\varepsilon_x(1 + \alpha_x^2)}{\beta_x} + \frac{\lambda}{L} \quad \Sigma_z'{}^2 = \frac{\varepsilon_z(1 + \alpha_z^2)}{\beta_z} + \frac{\lambda}{L}. \tag{15}$$

4.2. Application to Helios

Because of the chicane, the upstream and downstream undulator segments from Helios make their own footprint. Viewed at a 30 m distance from the source, assuming a typical value of $uhg = lhg = 15$ mm, the footprints from both undulator segments are horizontally spaced by 7.5 mm. Table 2 gives the total flux and polarization rates from any individual undulator segment for various settings of uhg, lhg and φ and harmonic of the radiation. The electron current is 200 mA and the electron energy is 6 GeV.

The polarization rates have been computed assuming a filament beam. There are various sources of depolarization, all of which contribute to reducing the value of R below 1. Non-zero emittance in an ideal undulator field induces a small depolarization. With the low emittance of the ESRF, this depolarization has been estimated using the code *Radia* (Chavanne & Elleaume, 1990) to give $R > 0.99$ on any harmonic below 3. Another contribution to depolarization comes from the variation of the fundamental with the transverse position (x,z) of the electron in the undulator. This phenomena occurs as a result of the non-uniformity of the peak fields around the central axis $(x,z) = (0,0)$. This effect has been estimated to give $R > 0.98$ at any setting of uhg, lhg and φ. Finally, field errors, the field from the chicane and that from adjacent bending magnets may also reduce the polarization rate.

5. Interaction with the electron beam

5.1. General

It is known from many synchrotron sources that undulators and wigglers can perturb an electron or positron beam stored in a ring. The typical perturbations are closed-

orbit displacements and tune shifts. A more severe effect can be a reduction of the beam lifetime. The magnetic field from Helios is much more complex than that of a conventional undulator and wiggler. A comprehensive new study has been performed by the author (Elleaume, 1992). The main results are summarized below. The computation starts from the Maxwell equations. One assumes that the electron does not pass through any current loop (the case for any permanent magnet or hybrid ID). As it crosses an ID, it experiences an angular kick (θ_x, θ_z), which can be expressed as

$$\theta_x = \frac{\partial \Phi}{\partial x} \quad \theta_z = \frac{\partial \Phi}{\partial z} \quad \Phi = \sum_{n=1}^{\infty} \Phi_n, \quad \Phi_n \propto \frac{1}{E^n} \quad (16)$$

where Φ is a function of the coordinates x and z at which the electron is injected in the ID. Second-order derivatives of Φ give the horizontal, vertical and skew focal distances F_x, F_z and F_c:

$$\frac{1}{F_x} = \frac{\partial \theta_x}{\partial x} \quad \frac{1}{F_z} = \frac{\partial \theta_z}{\partial z} \quad \frac{1}{F_c} = \frac{\partial \theta_x}{\partial z}. \quad (17)$$

Further derivatives give the so-called non-linear terms. The angular kick results in a closed-orbit displacement all over the ring. The r.m.s. spatial (angular) displacement of the closed orbit scaled to the r.m.s. natural size (divergence) is given by

$$\frac{\langle x^2 \rangle}{\sigma_{\beta_x}^2} = \frac{\langle x'^2 \rangle}{\sigma'^2_{\beta_x}} = \frac{\beta_x \theta_x^2}{8 \varepsilon_x \sin(\pi \nu_x)} \quad (18)$$

where ν_x is the betatron tune and σ_{β_x} and σ'_{β_x} are the betatron contributions to the beam size and angular spread. The same relationship applies in the vertical plane replacing x by z. The focusing induces a modification of the betatron functions all over the ring resulting in a modification of beam sizes and angular spread. The overall effect can be quantified in terms of a global betatron tune shift:

$$\delta \nu_x \simeq \frac{1}{4\pi} \frac{\overline{\beta_x}}{F_x} \quad \delta \nu_z \simeq \frac{1}{4\pi} \frac{\overline{\beta_z}}{F_z} \quad \delta \nu_c \simeq \frac{1}{4\pi} \frac{(\overline{\beta_x} \, \overline{\beta_z})^{1/2}}{F_c} \quad (19)$$

where $\delta \nu_c$ is the width of the coupling resonance and $\overline{\beta}_x$ and $\overline{\beta}_z$ are the beta functions averaged over the length of the ID. In addition to the tune shift, the betatron function changes all along the circumference. The maximum variation of the beta function is related to the tune shift by:

$$\frac{\delta \beta_x}{\beta_x} = \frac{2\pi \delta \nu_x}{\sin(2\pi \nu_x)} \quad \frac{\delta \beta_z}{\beta_z} = \frac{2\pi \delta \nu_z}{\sin(2\pi \nu_z)}. \quad (20)$$

5.1.1. First order.
At first order in $1/E$, Φ (m) and the angular kick θ_x, θ_z (rad) can be written as:

$$\Phi_1 = (0.3/E) \int_{-\infty}^{\infty} A_s \mathrm{d}s$$

$$\theta_x = (0.3/E) \int_{-\infty}^{\infty} B_z \mathrm{d}s$$

$$\theta_z = (-0.3/E) \int_{-\infty}^{\infty} B_x \mathrm{d}s \quad (21)$$

where A_s (T m) is the longitudinal component of the magnetic vector potential. In general θ_x and θ_z depend on x,z and the magnetic gap g. It is desirable to have $(\theta_x, \theta_z) = (0,0)$ for any gap inside a reasonably large region around $(x,z) = (0,0)$ since all derivatives of (θ_x, θ_z) versus x and z must be reasonably small to prevent extra linear or non-linear focusing (multipole). By a careful magnetic design, (θ_x, θ_z) can be made very small. The remaining contribution comes from the non-uniformity of the magnetization in the magnet blocks. The correction of the dipole contribution resulting from these imperfections can be made with horizontal and vertical coils. However, the remaining higher multipoles are much more difficult to correct in this way. An alternative is the multipole shimming performed routinely at ESRF, which removes all multipole components at any gap value without the need for any correction coil.

5.1.2. Second order.
Assuming the first order to be corrected, the second order contribution to Φ is

$$\Phi_2 = -\frac{1}{2}\left(\frac{0.3}{E}\right)^2 \int_{-\infty}^{\infty} \left[\left(\int_{-\infty}^{s} B_x \mathrm{d}s\right)^2 + \left(\int_{-\infty}^{s} B_z \mathrm{d}s\right)^2\right] \mathrm{d}s \quad (22)$$

where magnetic fields are expressed in T and distances in m. Of special interest is the case where the magnetic field is symmetrical with respect to horizontal and vertical planes intersecting along the central symmetry axis (the case of a conventional ID). The angle and skew focusing are zero along this axis, the lowest order non-zero derivatives of Φ are the horizontal and vertical focal lengths. Because of the Maxwell equations, they must obey the following relation

$$\frac{1}{F_x} + \frac{1}{F_z} = \left(\frac{0.3}{E}\right)^2 \left(\int_{-\infty}^{+\infty} B_x^2 \mathrm{d}s + \int_{-\infty}^{+\infty} B_z^2 \mathrm{d}s\right). \quad (23)$$

It is worthwhile noticing the difference from conventional first-order quadrupoles which have a focusing sum equal to zero. Another case of interest is a sinusoidal magnetic field for which Φ can be written independently of φ as

$$\Phi_2 = -5.7 \times 10^{-4} \left(\frac{\lambda_0}{E}\right)^2 L\left(\widehat{B}_x^2 + \widehat{B}_z^2\right) \quad (24)$$

where λ_0 is the ID period, L is the length of the ID and $\widehat{B}_x$ and $\widehat{B}_z$ are the peak horizontal and vertical magnetic fields. It is interesting to note the following relationship between the fundamental energy ε_1 and the potential Φ_2

$$\frac{1}{\varepsilon_1} = -8.06 \times 10^8 \frac{\Phi_2}{N} + \frac{\lambda_0}{0.0095 E^2} \quad (25)$$

Table 3

Horizontal (dx) and vertical (dz) r.m.s. closed-orbit displacement normalized to the r.m.s. beam size and betatron tune shifts for various settings of lhg, uhg and φ.

Case	lhg (mm)	uhg (mm)	φ (rad)	dz	dx	dν_z	dν_x	dν_c
1	15	15	0	−0.065	2.2×10^{-4}	5.0×10^{-4}	3.0×10^{-5}	5.2×10^{-7}
2	15	15	$\pi/2$	−0.065	2.7×10^{-4}	5.0×10^{-4}	2.8×10^{-5}	5.9×10^{-7}
3	15	15	$-\pi/2$	−0.065	1.8×10^{-4}	5.0×10^{-4}	3.3×10^{-5}	4.5×10^{-7}
4	15	∞	0	−0.17	3.8×10^{-16}	2.8×10^{-4}	-6.3×10^{-6}	1.8×10^{-18}
5	∞	15	0	0.11	1.4×10^{-4}	2.3×10^{-4}	8.4×10^{-5}	3.4×10^{-7}
6	10	10	0	−0.037	3.8×10^{-4}	1.4×10^{-3}	1.3×10^{-4}	1.1×10^{-6}

where N is the number of periods of the ID. This relationship applies to any periodic magnetic field (not necessarily sinusoidal). It means that the dependence of $1/\varepsilon_1$ and Φ_2 upon (x,z) is essentially identical. As discussed above, in conventional planar IDs, no angle is experienced by an electron injected on axis. The horizontal magnetic field is usually very small around the axis and the vertical peak field essentially depends on z. The main effect is then a vertical focusing and a small horizontal defocusing related to each other by (23).

5.2. Prediction for Helios

A single undulator section of Helios presents an undesirable feature in that the electron beam undergoes slight horizontal deviation if φ is varied between $-\pi$ and π. This feature is largely corrected by coupling two undulators with opposite polarization. The angle induced by one undulator is exactly compensated by the angle induced by the other undulator. The result is only a displacement of the trajectory between the entrance and exit. In the worst case this displacement is 1.6 μm. A closed-orbit distortion occurs due to this displacement, which is typically L/β_x smaller than that induced by a single undulator. Furthermore, as discussed in the section on polarization, Helios is intended to be operated in extreme cases where only the horizontal (vertical) magnetic field is present; this implies a distortion of the vertical closed orbit. A detailed analysis of the closed-orbit deviation and tune shifts as the three degrees of freedom are varied has been carried out taking into account the full three-dimensional field of the undulators and of the chicane. The $1/E^2$ contributions are summarized in Table 3.

This table has been computed with $\beta_x = 27$ m, $\beta_z = 13$ m, $\alpha_x = \alpha_z = 0$, $\varepsilon_x = 7$ nm, $\varepsilon_z = 0.7$ nm, $\nu_x = 36.2$ and $\nu_z = 11.3$, and a 6 GeV electron energy. dx (dz) is the ratio between the r.m.s. horizontal (vertical) closed-orbit distortion scaled to the r.m.s. beam size. The effects are small in absolute value; some of them are likely to be very difficult to measure. There is no significant variation *versus* phasing. Very small coupling is expected in all situations.

5.3. Measurement on Helios

Using four photon-position monitors sensitive to a few micrometers and placed at positions having a typical beta function of 30 m in both horizontal and vertical planes, closed-orbit distortion has been observed. The results are summarized in Table 4.

Table 4

Absolute closed-orbit displacement measured when varying lhg, uhg and φ.

	A	B	C
Horizontal	45 μm	27 μm	6 μm
Vertical	18 μm	5 μm	3 μm

Case A corresponds to a change of lhg between 50 and 11 mm while $uhg = 50$ mm and $\varphi = \pi/2$. Case B corresponds to a change of uhg between 50 and 11 mm while $lhg = 50$ mm and $\varphi = \pi/2$. Case C corresponds to varying φ between $\pi/2$ and $-\pi/2$ while $uhg = 15$ mm and $lhg = 15$ mm. Note that the field parameter that produces the most distortion is lhg (vertical magnetic field). The r.m.s. vertical (horizontal) closed-orbit distortion given by lhg in Table 4 is equal to 6% (4%) of the r.m.s. beam size. The closed-orbit displacement under a pure phase variation is very low and entirely due to the residual field integrals. The order of magnitude of the closed-orbit distortion is in good agreement with the expected values discussed earlier. The discrepancy between Tables 3 and 4 probably originates from the residual non-zero field integral (<30 μT m) and from the imprecise way of computing the r.m.s. of the closed-orbit deviation from only four randomly placed monitors. Note that Helios was run without any current in its correction coils. Powering these coils will probably reduce the closed-orbit distortion by a typical factor of 10. No measurable tune shift ($<1.0 \times 10^{-3}$) was recorded for any of the three cases.

6. Conclusions

Helios was installed on the ESRF storage ring in June 1993. As expected, the beam lifetime is not affected by the asymmetry of the field. The measured closed-orbit displacement is consistent with the residual field integral measurements and the prediction. A monochromator and a polarimeter are being installed to measure the spectrum and the polarization characteristics. A second helical undulator segment called Helios-2 is presently being measured and shimmed and is scheduled for installation on the ring before the end of 1994. Helios-2 is a single undulator (32 periods of 52 mm). The maximum field compatible with a 20 mm thick vacuum chamber is 0.14 T horizontal (0.22 T

vertical). By combining harmonics 1, 3 and 5, the photon energy range between 3.5 and 20 keV will be covered with highly flexible polarization. Helios has been designed in order to generate linear and/or circular polarization. Other exotic polarizations are sometimes envisaged by the users of the beamlines. I would like to mention the following generalization of the Helios concept. One can view Helios as a device which combines two orthogonal polarizations (horizontal and vertical) of the magnetic field to produce any other polarization orthogonal to the s_1 axis of a Poincarre sphere. This statement can be further generalized to the following. Any polarization described by a point belonging to a fixed big circle drawn at the surface of the Poincarre sphere can be generated by means of two magnet arrays whose magnetic field polarization corresponds to the axis orthogonal to the big circle. As a particular case, a device having linear polarization with variable direction in space can be built by combining an upper (lower) magnet array producing a right-handed (left-handed) circularly polarized magnetic field.

References

Born, M. & Wolf, E. (1987). *Principles of Optics*. Oxford: Pergamon Press.

Carr, R. (1993). SSRL ACD Note 127. SSRL, Stanford, California, USA.

Chavanne, J., Chinchio, E., Diot, M., Elleaume, P., Frachon, D., Marechal, X., Mariaggi, C. & Revol, F. (1992). *Rev. Sci. Instrum.* **63**(1), 317–320.

Chavanne, J. & Elleaume, P. (1990). ESRF Internal Report ESRF-SR/ID-90-46. ESRF, Grenoble, France.

Diviacco, B. & Walker, R. P. (1990). *Nucl. Instrum. Methods*, **A292**, 517–529.

Elias, L. R. & Madey, J. M. J. (1979). *Rev. Sci. Instrum.* **50**(11), 1335–1341.

Elleaume, P. (1990). *Nucl. Instrum. Methods*, **A291**, 371–377.

Elleaume, P. (1992). *Proceedings of the 3rd European Particle Accelerator Conference, EPAC 92*, 24–28 March 1992, pp. 661–663. Paris: Editions Frontieres.

Elleaume, P., Chavanne, J., Marechal, X., Goulon, J., Braicovich, L., Malgrange, C., Emerich, H., Marot, G. & Susini, J. (1991). *Nucl. Instrum. Methods*, **A308**, 382–389.

Goulon, J., Elleaume, P. & Raoux, D. (1987). *Nucl. Instrum. Methods*, **A254**, 192–201.

Kim, K. J. (1984). *Nucl. Instrum. Methods*, **219**, 425–429.

Kim, K. J. (1986). *Nucl. Instrum. Methods*, **A246**, 67–70.

Kincaid, B. (1977). *J. Appl. Phys.* **48**, 2684–2691.

Krinsky, S. (1983). *IEEE Trans. Nucl. Sci.* **30**, 3078–3082.

Moissev, M., Nikitin, M. & Fedorov, F. (1978). *Sov. Phys. J.* **21**, 332.

Onuki, H. (1986). *Nucl. Instrum. Methods*, **A246**, 94–98.

Pfluger, J. & Heintze, G. (1990). *Nucl. Instrum. Methods*, **A289**, 300–306.

Sasaki, S. (1993). *Nucl. Instrum. Methods*, **A331**, 763–767.

Schwinger, J. (1949). *Phys. Rev.* **75**, 1912–1925.

Yamamoto, S. & Kitamura, H. (1987). *Jpn. J. Appl. Phys.* **26**(10), L1613–L1615.